Modeling Study of a Flow Generated by the Local Imposition of Thermal Load on the Surface of a Water Body

A. Leousidis, Y. Savvidis, E. Keramaris*, G. Pechlivanidis
Department of Environmental Engineering, International Hellenic University, Sindos, 57400, Thessaloniki, Greece.
*to whom all correspondence should be addressed: e-mail: ekeramaris@ihu.gr

Abstract

This work aims to develop and apply a mathematical model for heating in the water body of an open channel via the local imposition of a thermal load on the water's surface. The study was supplemented with laboratory experiments. The mathematical simulation includes the processes of mass, temperature-density and momentum transport. The finite differences method was used, while momentum and mass conservation equations were applied. Regarding the laboratory experiments an open channel and a thermal radiation source were used. The research focused on the temperature distribution and the two-dimensional velocity field (XZ plane) along the channel, which is developed due to the temperature and waters' density differences. The numerical model results were compared with laboratory experiments and a good agreement was showed. The study showed that the process of advection was the prevailing factor of mass and temperature transport in relation with the diffusion process. In addition, the isothermal curve diagrams revealed the final length of the motion of heated masses when the phenomenon reaches steady and thermal equilibrium is achieved. Furthermore, under the influence of thermal load the motion of the heated mass was determined depending on the amount of heat imparted to the surface water.

Keywords: Open Channel; Laboratory Experiments; Numerical Comparisons; Experimental Comparisons; Heat and Mass Transfer

1. Introduction

The heating of the water surface in a water body and the subsequent study of the velocity field, temperature field and density field occur naturally in water reservoirs (e.g. lakes) and all aquatic ecosystems.

The present study investigates the heat transfer process and its effect on the fluid dynamics of the water of an open channel. More specifically, it captures the temperature distribution along the length of the channel. Then, the velocity field was determined.

Wang et al. (2005) studied the simulation of turbulent flow in an open channel including heat transfer and large eddy simulation. They used boundary conditions to maintain a constant temperature flux on the free surface and investigated the heat transfer behavior in the turbulent flow of the open channel. Three-dimensional (3D) Navier-Stokes and energy equations were used. The results were compared with data of the literature and the agreement was very good.

Fan et al. (2009) investigated, by means of computational fluid dynamics (CFD) calculations, the heat loss that causes transient fluid flow during cooling. They presented the effects of thermal stratification in a vertical cylindrical hot water tank. The distribution of the heat loss coefficient in different parts of the tank was investigated. It was observed that natural buoyancy was created, which caused a downward flow along the side walls of the tank.

Liu et al. (2009) studied heat transfer through a three-dimensional (3D) numerical simulation focusing on a wave traveling along an open channel with turbulent flow. The Navier-Stokes and energy equations were considered. Fluctuations of the heat transfer were found depending on the periods of the wave. The simulations showed the effects on turbulent channel flow and heat transfer.

Tang et al. (2009) developed a one-dimensional (1D) open-channel model to analyze the temperature response to unsteady non-uniform flow at various channel points, such as the free surface, edges and bed. The model considers upstream and lateral flow variability and boundary

conditions. The solutions concern practical problems such as an inflowing stream upstream of a dam or wastewater released into a water receiver.

Anibas et al. (2010) studied the simulation of seasonal and spatial flow patterns with the thermal mapping method in a river section. The interaction of groundwater and surface water was examined by developing an one-dimensional (1D) heat transfer model to estimate vertical fluxes. The study's results showed that summer and winter seasonal streamflow estimates can be derived with minimal data input and simulation effort. Finally, the advanced thermal method is more cost-effective, simple, and fast, so it is recommended to identify zones of interest in groundwater-surface water interaction.

Peddisetty et al. (2016) studied the thermal stratification in nanofluids, which was developed and caused heat loss to the environment. The increase in the thermal stratification parameter had important effects on the velocity profiles and the temperature set in the nanofluids. Furthermore, the increase in the nanoparticle volume fraction enhanced the temperature and simultaneously decreased the velocity of the nanofluids.

Savvidis et al. (2017) investigated numerically and experimentally, the optimal design of the entrance of a fish refuge lateral to the main flow of an open channel. Mathematical simulations were based on the development and application of a two-dimensional (2D) hydrodynamic model and a three-dimensional (3D) sediment transport model. A comparison between the physical and the mathematical model ensured the validity of the model and the results led to the optimal technical design of the fishing shelter.

Koue et al. (2018) developed a three-dimensional (3D) hydrodynamic model to study the flow and thermal stratification field in a lake in Japan. The application of the model allowed for the analysis of the stratification structure in the lake with the seasonal changes over four years. The model results were in good agreement with the field data.

Chuang et al. (2019) study was carried out on the effect of heat caused by nuclear waste on lakes. The research focused on the transfer of boiling heat (bubble formation) to the fluid. The mathematical model developed for the research showed that the diameter and frequency of departure of the bubbles are increased by the orientation of heating from the nuclear site to the lake. Additional information and validation of boiling transfer models shall also be provided.

Kalinowska (2019) studied the problems associated with the spread of thermal pollution in rivers. An attempt was made to predict the rise in water temperature. Specific emphasis was given to the water-air heat exchange, which was examined. For this study, a mathematical model was used, approximating heat exchanges with the environment and how heat pollution is affected using appropriate temporal and spatial scales. The results showed that the intensity of solar radiation significantly affects the results over time, depending on the existence of clouds. In addition, the effect of the riverside area with vegetation was considered.

Benhamadouche and Manceau (2020) conducted a computational study concerning the simulation of heat flow and transfer in a blade array in a staggered industrial configuration. The stream was reproduced in various Reynolds numbers. The application of mathematical models led to velocity fields and turbulence due to momentum and heat mixing.

Kirkpatrick et al. (2020) used a numerical simulation of a thermally stratified flow model. The simulation was performed considering initially steady-state radiative heating. The thermal radiation was then reduced and a constant uniform cooling flow was applied to the surface. The result of the model simulation accurately gives the rate of delamination as well as the necessary time. In this way, the evolution of the internal structure of the turbulent flow field is destroyed.

Amjad et al. (2021) studied the heat transfer in a nanofluid flow under a magnetic field and thermal radiation in a narrow channel. They analyzed the flow characteristics and heat transfer rate, as well as the effects of variations in Hartmann number, Strouhal number, Prandtl number, and thermal radiation parameter. The equations governing these conditions are solved

numerically using the finite element method. Laminar flow simulations are performed in a two-dimensional (2D) system.

Aglawe et al. (2021) studied the prediction of heat dissipation to cool electronic systems. This study presents a mathematical model to determine a microchannel's heat transfer coefficient. The results showed that the thermal conductivity of the copper and the hydraulic diameter of the micro-channel play a critical role in determining the heat and transfer coefficient, which in turn affects the micro-channel cooling.

Cánovas et al. (2021) used a 2D mathematical simulation to study the transfer of heat in a flow based on the density of porous media. Based on the network simulation method, the developed mathematical model provided steady-state patterns and reliable results. It was observed that the transfer of heat depends on the Rayleigh Number and the values of the hydrological, thermal, and geometric parameters.

Issaev et al. (2021) investigated the flow of open channels through numerical simulations in a time-varying turbulent fluid. Three different mixing zones were observed and divided into transient values of the Froude number. Also, the study concerns the parameterization of flow mixing with varying energies within the stratified flow of the channel. The study found that after an initial transitional period of vortex adaptation, turbulent flow in the channel leads to the formulation of different mixing layers. In addition, buoyancy leads to a simple balance between shear forces and inertia. The model results contribute significantly to the study of stratified flows.

Rotich et al. (2021) developed a mathematical model to study the turbulent, non-uniform, and Newtonian flows of fluids in an open channel of parabolic cross-section. The MATLAB software was used to solve equations using the finite differences method. The study aimed at flood-protection channels such as those used for irrigation of cultivated land.

Savatora et al. (2024) developed a mathematical model using differential equations. The purpose was to determine the operation of a cost-effective hot water heating system within a cylindrical tank. The goal was to calculate the time for the water to reach the desired temperature given the power of the heating element and the size of the water tank.

Previous studies cover a wide spectrum of research related to the present study. More specifically, according to many earlier studies, mathematical models simulated field or laboratory physical processes and were mainly verified by literature data.

Kalvan et al. (2024) evaluated the effectiveness of Support Vector Machine (SVM) and Decision Tree Techniques (DTT) in the context of hydroponic tomato cultivation using the Deep Water Culture (DWC) method. These methods were tested in a hydroponic DWC system to predict tomato growth, production, and quality. SVM had better precision in some circumstances, while DTT was easier to interpret and apply.

Venkatraman et al., (2024) created a reliable and precise deep learning model, the ODD-RecurFlowNet, for the effective prediction and classification of water quality. They used sophisticated methodologies to achieve the model's objectives. On the water quality prediction dataset high performance and maximum accuracy was achieved.

Finally, Suresh et al. (2025) implemented appropriate treatment strategies for the Wastewater recycling. The main purpose was to transform polluted ponds into clean water sources through real-time monitoring and efficient treatment by tracking water quality parameters such as pH, dissolved oxygen, turbidity, and biological oxygen demand using plotted IoT sensors. A new algorithm was proposed which achieved a very good accuracy and precision, highlighting its robustness in detecting and treating water contaminants in real-time.

In this study, the developed mathematical model is validated and confirmed by the experimental results of Leousidis et al. (2022), which were conducted in an open channel of a

laboratory. The effect of the thermal load, locally imposed on the surface of a waters' body is exclusively investigated.

2. Computational Model

2.1. Materials and Methods

The main objective of this study was the development and the application of a mathematical model for the effect of local heating of the water's surface in an open channel. The Fortran programming language and the Surfer program were used for the production and visualization of the results.

The study was carried out for flow depths (h) of 5 and 15 cm. The channel was 10 m long. The location of the thermal load is given in figure 1.

Spatial resolution was selected with d_x=10 cm along the X axis and d_z=1 cm along the vertical Z axis. Thus, on the XZ plane, a grid was constructed where the maximum number of cells along the X-axis was i_m=100 while the maximum number of cells along the Z-axis was k_m=10. So, the grid that was used consisted of 1000 computational cells (i_m x km=1000). The time step dt, was 0.005 seconds.

The differential equations that were solved using the finite difference method are given below: First, the equation of conservation of momentum in the X-axis (equilibrium equation of forces) is used to calculate the velocity u.

$$\frac{\partial u}{\partial t} + u\frac{\partial u}{\partial x} + w\frac{\partial u}{\partial z} = -g\frac{\partial}{\partial x} - \frac{1}{\rho_0}\frac{\partial \zeta}{\partial x} + D_H\frac{\partial^2 u}{\partial t} + D_V\frac{\partial^2 u}{\partial z^2} \quad (1)$$

where:

u: water velocity in the horizontal direction (X-axis),

ζ: free surface elevation from the horizontal still water level

D_h: horizontal momentum diffusion coefficient,

D_v: vertical momentum diffusion coefficient,

g: acceleration of gravity

t: time

The equation of mass conservation (continuity equation) is used to calculate the velocity w.

$$\frac{\partial w}{\partial z} + \frac{\partial u}{\partial x} = 0 \quad (2)$$

where:

u: water velocity in the horizontal direction (X-axis),

w: water velocity in the vertical direction (Z-axis)

The depth-averaged velocity U is derived from the depth-integrated u velocities:

$$U = \frac{1}{h} \int u \, dz \quad (3)$$

The equation mass conservation (continuity equation), expressed as follows, is also used to calculate the variation of the water surface level Z (from the mean water level):

$$\frac{\partial \zeta}{\partial t} = -h \frac{\partial U}{\partial x} \quad (4)$$

where:

ζ : variation of the surface level from the mean water level,

U: integrated depth-averaged water velocity in the horizontal direction (X-axis),

t: time

The hydrostatic equation is applied to calculate the pressure P:

$$\frac{\partial \mathrm{P}}{\partial \mathrm{z}} = \rho \mathrm{g} \quad (5)$$

where:

P: pressure,

ρ : water density,

g: acceleration of gravity

The equation of turbulent diffusion of a substance (mass – density) is also applied to calculate the density ρ of water:

$$\frac{\partial \rho}{\partial t} = -\frac{\partial u\rho}{\partial x} - \frac{\partial w\rho}{\partial z} + SD_H \frac{\partial^2 \rho}{\partial x^2} + SD_V \frac{\partial^2 \rho}{\partial z^2} \quad (6)$$

where:

ρ: water density,

u and w: components of water velocities in the horizontal and vertical directions, respectively, as defined above,

SD_H: mass (dye) horizontal diffusion coefficient (dye),

SDv: coefficient of vertical diffusion coefficient (dye).

An important parameter is the equation of water density ρ and temperature T that was used in the laboratory experiments (Leousidis et al. 2022):

$$\rho = -0.00022 \cdot T + 1.0013 \quad \rightarrow \quad T = -(\rho - 1.0013)/0.00022 \quad (7)$$

where:

ρ: water density

T: temperature

2.2. Surface boundary conditions

The density at the source of heating area $\rho = \rho_\tau$

The temperature values at each channel cross-section on the free surface of the water measured on site are $\rho=\rho_{\tau ex.}$

In case there is no information about measured temperatures on the free surface water, the following equation is activated:

$$\frac{\partial^2 \rho}{\partial z^2} = 0 \quad (8)$$

The velocity values are computed according to the following equations:

$$\frac{\partial u}{\partial z} = 0 \quad (9)$$

$$\frac{\partial w}{\partial z} = 0 \quad (10)$$

The following paragraphs apply boundary conditions to the channel's solid boundaries.

2.3. Bottom boundary conditions

Concerning the bottom of the channel, the shear stress is computed by applying the equation 11:

$$\frac{\tau_b}{\rho} = C_b * u^2 \quad (11)$$

where:

τ_b: bottom shear stress,

ρ: water density,

C_b: bottom friction, coefficient

u: flow velocity near the bottom,

The channel bottom friction coefficient is calculated based on the following.

Von Karman relation:

$$C_b = \left[\frac{0.4}{\left(\log\left(\frac{h}{z_0}\right)-1\right.}\right]^2 \quad (12)$$

where:

$z_o = 0{,}03 \text{ x } k_s = 0{,}03 \cdot 0{,}0000015 = 4{,}5 \cdot 10^{-8}$

k_s: average roughness of the material of the bottom = 0,0000015 m (Tsakoyiannis, 2000).

$$D_v \frac{\partial u}{\partial z} = C_b * u^2 \quad (13)$$

$$w = 0 \quad (14)$$

$$\frac{\partial^2 \rho}{\partial z^2} = 0 \quad (15)$$

where:

ρ, u, w, D_v as described above

2.4. Lateral boundary conditions (left/ beginning and right/ending solid boundaries of the channel)

Concerning the lateral solid boundaries of the channel i.e. the walls, the shear stress is computed applying the following equations:

$$u = 0 \quad (16)$$

$$\frac{\partial^2 \rho}{\partial x^2} = 0 \quad (17)$$

where:

ρ, u as described above

2.5. Momentum and Mass Diffusion Coefficients

It is well known that transport of mass and momentum is realized through two parallel mechanisms, advection and diffusion. Emphasis should be given to the diffusion of the substance because it affects the velocity field. The determination of diffusion coefficient is thus a necessary step for the description of water circulation. Rodi (2000) describes a detailed study of momentum and mass diffusion. However, in this research, some simple relations for determining momentum and mass horizontal and vertical diffusion coefficients were used. For this purpose, some characteristic dimensions were derived from the laboratory experiments. More specifically, the calculation of the diffusion coefficients is described below.

The horizontal momentum diffusion coefficient D_H was derived from the following equation (Koutitas, 1996).

$D_H = a \cdot L^{4/3}$ (18)

where:

a = 0.01 and L characteristic length of flow development (cm) and D_H in cm^2/s

The vertical diffusion coefficient of momentum D_V was calculated by the following relationship (O' Brien, 1985):

$$D_V = \frac{\Delta z^2}{\Delta x^2} * D_H \quad (19)$$

where:

Δx: spatial step in the horizontal direction, and Δz is the spatial step in the vertical direction.

The horizontal and vertical diffusion coefficients of mass, SD_H, and SDV, respectively, were assumed to be equal to the momentum diffusion coefficients.

3. Results

3.1. Basic Outline of the Experiment (Model and Laboratory Experiments)

The following solution scenarios are presented using the mathematical model for a 5 and 15 cm flow depth (i.e. h_5 = 5 cm and h_{15} = 15 cm). The numerical results i.e. the model outputs are compared with the corresponding experimental results. The main parameters considered for the experiments are:

T_o: initial water temperature,

T_{su}: water surface temperature below the heat load source,

Experimental setup location (thermal load)

The velocity filed, i.e. u and v velocity components as well as temperatures along the channel result from the model application. The horizontal and vertical diffusion coefficients, D_H and

D_V respectively, are computed from the velocity values as well geometrical parameters as described in the previous section.

The data according to the corresponding experimental measurements are presented (Table 1).

3.2. Results of Mathematical Simulation

The model results based on the data in Table 1 are presented in figures 2- 21. These results correspond to the velocity field as well as the isothermal curves along the channel on XZ plane. The velocity and temperature fields along the channel, for flow depth 5 cm and experiment 1 are showed in figures 2 and 3, for flow depth 5 cm and experiment 2 are showed in figures 4 and 5, for flow depth 5 cm and experiment 3 are showed in figures 6 and 7, for flow depth 5 cm and experiment 4 are showed in figures 8 and 9, for flow depth 5 cm and experiment 5 are showed in figures 10 and 11, for flow depth 15 cm and experiment 1 are showed in figures 12 and 13, for flow depth 15 cm and experiment 2 are showed in figures 14 and 15, for flow depth 15 cm and experiment 3 are showed in figures 16 and 17, for flow depth 15 cm and experiment 4 are showed in figures 18 and 19 and for flow depth 15 cm and experiment 5, are showed in figures 20 and 21.

All the model runs concerned the hydrodynamics that refer to steady state flow conditions. A characteristic trend of the water moving from deeper layers towards to the surface where the thermal load was posed is observed. Furthermore, two eddies are developed on either side of the area below the thermal load.

3.3. Laboratory experiments and comparison with model results

The diagrams of the velocity fields (see figures 22 and 23) and the related curves allowed for the calculation of the length of the thermal wedge; this was achieved by determining the point where flow velocities are minimized (values close to zero).

Also, it was found that the length of motion of the mass under the influence of heating is proportional to the amount of thermal load imparted to the surface of the water. In addition, isothermal curves developed from the source to the free surface of the water. Furthermore, it was found that the length of the thermal wedges, apart from the direct relation to the amount of load delivered by the source, it is also depended on the difference in temperature ΔT and flow depths, h. The mean velocities of the diagram result under the influence of different thermal loads T_1, T_2, T_3, T_4 and T_5 as shown in figures 22 and 23.

According to the comparative results of the values of the velocity fields in Tables 2 and 3, a quite satisfactory convergence of the experimental results with those of the mathematical model was found.

The u-velocity diagrams resulting from the mathematical model and the experimental results are given in figures 24 to 33. On these diagrams (figures 24 - 33), the continuous lines that correspond to the fitted curves resulted from several points, i.e., values calculated numerically or experimentally. More specifically, the blue lines resulted from the red square points corresponding to the laboratory experiments. In contrast, the yellow lines resulted from the small blue rhombuses, which correspond to the velocity values computed by the numerical model.

4. Discussion

The mathematical model, developed and applied for the different cases of numerical experiments, seems to give very satisfactory results in comparison with the corresponding laboratory experiments. The comparison concerned the flow velocities (Tables 2 and 3) as well as the temperature field (isothermal curves). It was observed that the mathematical model

slightly underestimates the values of the current velocities concerning the case of 5 cm flow depth, in contrast to the flow depth of 15 cm. More analytically, the slight differences between the results of model and laboratory experiments are possibly due to the fact that all numerical experiments used the same spatial analysis, which means that in the case of lower flow depths of 5cm there was less number of layers in relation with higher flow depths.

Concerning the water velocities, it seems that the flow which is developing on the water surface is directed from the water surface area under the source towards the neighboring waters away from the source. It is noted that the open channel is bounded by walls at both ends and the flow is forced to recirculate. In this way, water from lower layers move upwards to the surface area under the source and then a horizontal surface flow away from the source starts to develop, leading to the formation of a clockwise (i.e. anticyclonic) eddy on XZ plane at the right part of the channel and an anticlockwise (i.e. cyclonic) eddy at the left side of the channel. These waters' movements were confirmed by the laboratory experiments. The motion of rhodamine for the case of experiment 4 and water depth 15 cm is shown in figure 34 below as a characteristic example, which seems to be in line with the model results (figure 18).

The above water circulation can be reversely related to the circulation which results in case of a cooling an area of the water surface. It is well known that in this case water masses of the surface begin to sink in lower layers. The present experiments show that heating an area of water surface cause an upward movement from water of lower layers. Of course, another more focused study of cooling waters' surface can be realized for the completion of an integrated study of heating and cooling the surface of a water system.

According to the experimental measurements (Table 4), the initial temperature of the water T_w (before the effect of heat), also the temperature T_0 of the free surface at the position –location under the influence of the external thermal load, as well as the temperature T_{eq} of the water when thermal equilibrium is achieved, the length of the thermal wedge L (thermal mass

transfer) and finally the thickness b of the thermal mass-produced at the initial position of the experiment are recorded in Table 4. The measurements of the thermal wedge and thermal mass thickness were derived from isothermal curve diagrams and velocity diagrams (Leousidis, 2022).

According to Table 4, the Peclet number is greater than 1 (Pe>1). Consequently, it is documented that the transport of water masses and temperature is mainly developed by advection, i.e., the advection process prevails over diffusion. Under the influence of heat load, the transfer of energy is accomplished by radiation.

5. Conclusions

In this paper, the flow generated by the imposition of thermal load on a particular area of the surface of an open channel was studied using modeling tools. More specifically, an integrated study was carried out, based on the successful combination of numerical modeling (which constituted the main body of the present research) with laboratory experiments that confirmed the model's validity and also completed the study providing added value to the whole research work. In more detail, the experimental research produced an equation for determining the length of mass motion under the influence of heat load. Based on this approach, the study of the length of a pollutant's movement in a water recipient and the determination of its self-purification can follow.

The basic output of this specific research was the information about the temperature distribution along the water body of the channel as well as the velocity field which was developed. In more detail, according to the above presented model results, after establishing equilibrium conditions, the isotherms show clearly the trend to be parallel with the water surface with increased values near the surface and decreased values downwards, as expected. As far as the velocity field is concerned, a characteristic upward motion of deeper water is

observed in the area under the thermal load, while two eddies, one anticyclonic, to the right of the thermal source and another cyclonic, to the left of the thermal source, are developed when the flow reaches steady state conditions. The aforementioned model results were confirmed by the laboratory experiments i.e. the model output referring to the flow velocities as well as the temperature field seem to be very close to the measurements and recordings of the relevant flow and water parameters in the channel, which ensures the model's validity.

Concerning the improvement of the model's performance and accuracy, the use of a variable discretization of the computational domain can be proposed i.e. increase of the number of cells close to the surface and close to the bottom of the channel.

According to the above presented model results, after establishing equilibrium conditions, the isotherms show clearly the trend to be parallel with the water surface with increased values near the surface and decreased values downwards, as expected. As far as the velocity field is concerned, a characteristic upward motion of deeper water is observed in the area under the thermal load, while two eddies, one anticyclonic, to the right of the thermal source and another cyclonic, to the left of the thermal source, are developed when the flow reaches steady state conditions.

Similar studies concerning the modeling work have conducted recently, focusing however on different aims. More, specifically Ji et al. (2024) developed a mathematical model to predict dissolved oxygen (DO) distribution and oxygen transfer rate with an ultimate aim the maximization of the performance of a Recirculating Aquaculture System. They used in their methodology several information and technical approaches like aeration flow rates, DO measurements, water quality parameters, as well as hydrodynamic simulations. Moreover, Qiu et al. (2024) attempted successfully to address knowledge gaps related to the systematic identification and calibration of Computational Fluid Dynamic (CFD) simulation models for

the contribution to the study of the physical-chemical hydrodynamics of activated sludge reactor design and operation, and their impact on Nitrous Oxide (N_2O) emission.

The present mathematical model can be used in future research with different scenarios, such as adding resistance from vegetation as well as the existence of salinity. Furthermore, the mathematical model that was developed can be used to identify the optimal water intake location in a water basin, as high-temperature supply should be avoided. Moreover, the presented model can be applied to studies concerning protection of the environment from waste pollution in water receivers, as it can determine the length of transport of the pollutant load. From the practical point of view, the present research can indicatively be applied:

- in a water basin for water supply use of an area. Determining the correct placement of the water abstraction is valuable so that high-temperature water is not drained,
- in cases where hot or cold liquid masses discharged to a recipient; the maximum length of these hot or cold-water masses can be determined,
- for the knowledge of the height differences in water temperature of the heated basin from solar radiation.
- for the study of the dispersion of wastewater pollutants to water recipients, e.g., lakes, seas, etc.
- in cases that the temperature of the water is a determining factor for the study of a freshwater ecosystem. Its investigation is imperative in a changing climate environment.

Conflict of Interest

On behalf of all authors, the corresponding author states that there is no conflict of interest.

Authors Contribution

All authors contributed to the study conception and design. Material preparation, data collection and analysis were performed by Leousidis A., Savvidis Y., Keramaris E. and Pechlivanidis G. The first draft of the manuscript was written by Alexandros Leousidis and all authors commented on previous versions of the manuscript. All authors read and approved the final manuscript.

References

[1] Amjad, A., Zainb, B., Cullnaz, S., Zaheer, A. and Muhammad, U. (2021). Numerical Simulation of the Thermally Developed Pulsatile Flow of a Hybrid Nanofluid in a Constricted Channel. *Energies 14,* 2410.

[2] Aglawe, K.R., Yadav, R.K., Thool, S.B. (2022). Development of a mathematical model for prediction of heat transfer coefficient in micro-channel heat sink. *Materials Science and Mathematics for Advanced Technology, proceedings 54*, 753–757.

[3] Anibas, C., Buis, K., Verhoeven, R., Meire P. and Batelaan O. (2010). A simple thermal mapping method for seasonal spatial patterns of groundwater–surface water interaction, *Journal of Hydrology 397(1-2),* 93–104.

[4] Benhamadouche, S., Afgan, I., Manceau, R. (2020). Numerical Simulations of Flow and Heat Transfer in a Wall-Bounded Pin Matrix. Flow. *Turbulence and Combustion 104,* 19–44.

[5] Cánovas, M., Alhama, I., García, G., Trigueros, E. and Alhama F. (2017). Numerical Simulation of Density-Driven Flow and Heat Transport Processes in Porous Media Using the Network Method. *Energies, 10*, 1359.

[6] Chuang, T.J., Chang, Y.H., Ferng, Y.M. (2019). Investigating effects of heating orientations on nucleate boiling heat transfer, bubble dynamics, and wall heat flux partition boiling model for pool boiling. *Applied Thermal Engineering 163*, 114358.

[7] Fan, J., Furbo, S. (2009). Thermal Stratification in a hot water tank established by heat loss from the tank. proceedings of the ISES Solar Word Congress Renewable Energy Shaping our Future.

[8] Issaev, V., Williamson, N., Armfield, S.W. and Norris S.E. (2022). Parameterization of mixing in stratified open channel flow. *Journal of Fluid Mechanics 935*, A17.

[9] Ji, M., Ye, Z. and Li, H. (2024). Performance evaluation and mathematical model of pipeline diffused aeration for recirculating aquaculture system. Aquacultural Engineering 105, 102410.

[10] Kalinowska, M. B. (2019). Effect of water–air heat transfer on the spread of thermal pollution in rivers. *Acta Geophysica 67*, 597–619.

[11] Kirkpatrick M.P., Williamson, N., Armfield, W.S., Zecevic, V. (2020). Destratification of thermally stratified turbulent open-channel flow by surface cooling. Published online by Cambridge University Press.

[12] Koue, J., Shimadera, H., Matsuo, T. and Kondo A. (2018). Evaluation of Thermal Stratification and Flow Field Reproduced by a Three-Dimensional Hydrodynamic Model in Lake Biwa, Japan. *Water 10,* 47.

[13] Koutitas, C. (1996). Introduction to coastal engineering and port works, Ziti press, Thessaloniki Greece.

[14] Koutitas, C, Scarlatos, P. (2015). Computational Modelling in Hydraulic and Coastal Engineering, CRC Press.

[15] Leousidis, A., Keramaris, E, Pechlivanidis, G. and Savvidis, I. (2022). Experimental study of the effects of heating or cooling on the water surface in an open channel. International

conference EWaS5, Water security and safety Management: emerging threats or new challenges, Napoli, Italy.

[16] Leousidis, A., Pehlivanidis, G., Keramaris, E. and Savvidis, I. (2022). Participation in the 15th EHE & APTH Conference on the theme: ¨Excellent water¨ Thessaloniki, with the title of the article: 'Study of Thermal Wedge due to temperature field changes.

[17] Leousidis, A. (2022). Experimental and computational determination of fluid (water) flow velocities in an open channel due to temperature changes, University of Thessaly, Department of Civil Engineering, PhD thesis.

[18] Liu, N.S., Wang, L., Lu X.Y. (2009). Turbulent open channel flow with heat transfer subjected to the control of a spanwise travelling wave, *International Journal of Heat and Mass Transfer 52,* 4375–4385.

[19] Qiu, Y., Ekström, S., Valverde-Pérez, B., Smets, B. F., Climent, J., Domingo-Félez, C. and Plosz, B. G. (2024). Numerical modeling of surface aeration and N2O emission in biological water resource recovery. *Water Research 255,* 121398.

[20] Suresh, M., Rajendran, S., Selvanarayanan, R., Gowri, S. (2025). Wastewater Recycling Integration with IoT Sensor Vision for Real-time Monitoring and Transforming Polluted Ponds into Clean Ponds using HG-RNN. *Global NEST Journal 27(4),* 06758.

[21] O' Brien, J.J. (1985). Advanced Physical Oceanographic Numerical Modelling', NATO ASI Series. Sringer-Science+Business Media, B.V, Banyuls-sur-mer, France.

[22] Pavan K. B., Surendran, R., Sumathy, K. (2024). Comparative of SVM and Decision Tree Techniques for Predicting Hydroponic Tomato Growth and Yield Using Deep Water Culture. International Conference on Innovation and Intelligence for Informatics, Computing, and Technologies (3ICT), Sakhir, Bahrain, 2024, 705-710.

[23] Peddisetty, N.C. (2016). Effects of thermal stratification on transient free convective flow of a nanofluid past a vertical plate. Pramana – *Journal of Physics 87*, 62.

[24] Rotich, F.K., Maremwa, J.M. and Kandie, J.K. (2021). Mathematical modeling of flow of fluids in an open channel of parabolic cross-section. International *Journal of Statistics and Applied Mathematics; 6(3),* 76-82.

[25] Savvidis, I., Keramaris, E., Pechlivanidis, G. and Koutitas, C. (2017). Optimum Design of the Entrance of a Fishpond Laterally to the Main Stream of an Open Channel, *Environmental Science and Pollution Research, 24 (25),* 20122-20133.

[26] Savatora, V. and Talonov, A. (2024). Teaching differential equations through modelling: hot water heater. *International Journal of Mathematical Education in Science and Technology, 55 (2)*, 235-263.

[27] Tang, S.H. and Keen, R.T. (2009). Analytical Solutions for Open-Channel Temperature Response to Unsteady Thermal Discharge and Boundary Heating. *Journal of Hydraulic Engineering, 135 (4).*

[28] Tsakoyiannis I. (2000). Fluid Mechanics, Paratiritis, Thessaloniki.

[29] Venkatraman, M., Surendran, R., Srinivasulu, S., Vijayakumar, K. (2024). Water quality prediction and classification using Attention based Deep Differential RecurFlowNet with Logistic Giant Armadillo Optimization. *Global NEST Journal 27(4),* 06758.

[30] Wang, L., Dong Y.H., Lu X. (2005). An investigation of turbulent open channel flow with heat transfer by large eddy simulation, *Computers and Fluids 34*, 23–47.

Table 1. Mathematical code solving elements

Flow Depth (cm)	T_0 (^{0}C)	T_{su} (^{0}C)	D_H (m^2/s)	D_V (m^2/s)
h_5, exp.1	21.0	21.0	0.0008	0.000008
h_5, exp.2	19.9	19.9	0.0022	0.000022
h_5, exp.3	20.2	20.2	0.0032	0.000032
h_5, exp.4	20.3	21.3	0.0048	0.000048
h_5, exp.5	20.4	20.4	0.0060	0.000060
h_{15}, exp.1	18.8	22.5	0.0012	0.000012
h_{15}, exp.2	16.0	22.0	0.0018	0.000018
h_{15}, exp.3	16.0	22.0	0.0029	0.000029
h_{15}, exp.4	15.4	23.5	0.0040	0.000040
h_{15}, exp.5	15.4	24.5	0.0060	0.000060

Table 2. Comparative results of values of flow depth velocity fields h=5 cm

	Based on experiments in the laboratory channel			
	Velocity (cm/sec)		T_o	T_{su}
	U_{min}	U_{max}	(°C)	(°C)
Experiment 1	0.011	0.130	21.0	29.5
Experiment 2	0.010	0.160	19.9	31.5
Experiment 3	0.010	0.170	20.2	31.5
Experiment 4	0.010	0.200	21.3	34.0
Experiment 5	0.010	0.220	20.4	35.0

	Based on numerical experiments from its application			
	Velocity (cm/sec)			
	U_{min}	U_{max}	Deviation value U'_{max}	Deviation value U'_{min}
Experiment 1	0.011	0.135	4%	9%
Experiment 2	0.010	0.160	0%	0%
Experiment 3	0.010	0.170	0%	0%
Experiment 4	0.010	0.200	0%	0%
Experiment 5	0.010	0.220	0%	0%

Table 3. Comparative results of values of flow depth velocity fields h=15cm

	Based on experiments in the laboratory channel			
	Velocity (cm/sec)		T_o	T_{su}
	U_{min}	U_{max}	(°C)	(°C)
Experiment 1	0.011	0.090	18.9	22.5
Experiment 2	0.010	0.130	16.0	22.0
Experiment 3	0.010	0.140	15.6	23.0
Experiment 4	0.011	0.145	15.4	23.5
Experiment 5	0.010	0.170	15.4	24.5

	Based on numerical experiments from its application			
	Velocity (cm/sec)		Deviation value U'_{max}	Deviation value U'_{min}
	U_{min}	U_{max}		
Experiment 1	0.010	0.100	11%	9%
Experiment 2	0.010	0.130	0%	0%
Experiment 3	0.010	0.140	0%	0%
Experiment 4	0.010	0.150	3%	9%
Experiment 5	0.010	0.170	0%	0%

Table 4. Determination of dimensionless Peclet number (Pe) under heat load

Experiment	thermal wedge length L (cm)	diffusion of substance D (cm^2/s)	The average velocity U(cm/s)	Pe ($U_{av}xL$)/ D
H15_exp.1	200	11.7	0.07	1.20
H15_ exp.2	280	18.3	0.10	1.53
H15_ exp.3	400	29.5	0.10	1.36
H15_ exp.4	500	39.7	0.12	1.51
H15_ exp.5	680	59.8	0.13	1.48
H05_ exp.1	150	8.0	0.08	1.51
H05_ exp.2	320	21.9	0.08	1.17
H05_ exp.3	430	32.5	0.10	1.32
H05_ exp.4	580	48.4	0.10	1.20
H05_ exp.5	680	59.8	0.14	1.59

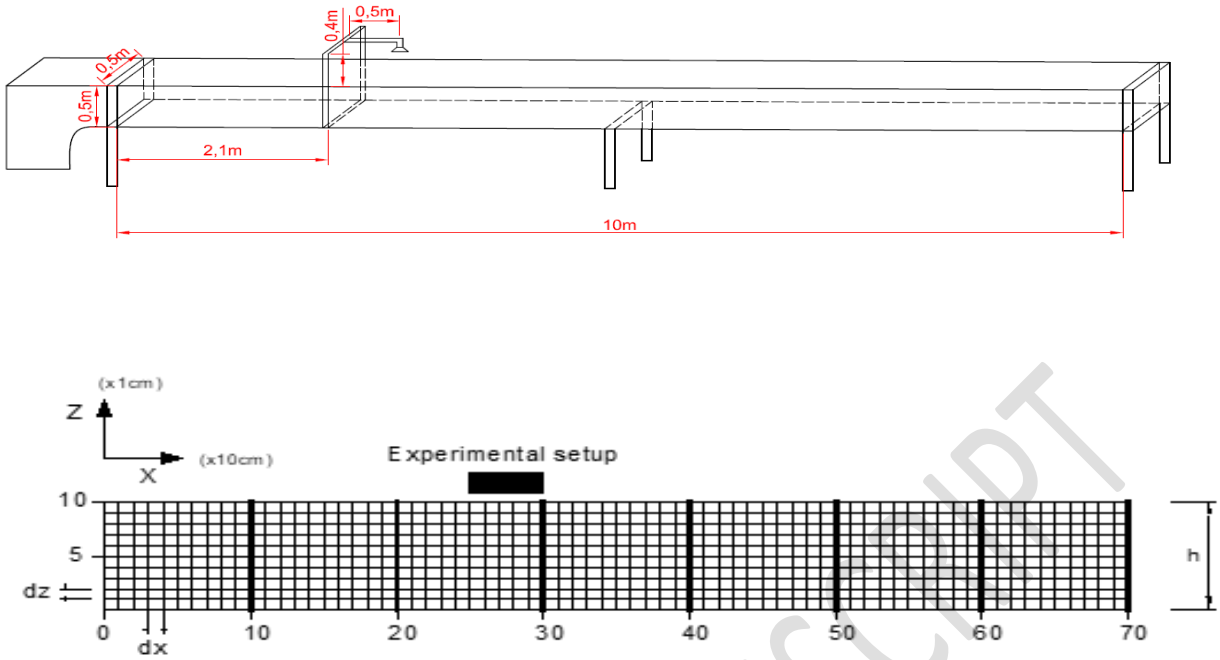

Figure 1. Schematic representation of calculation canvas generation with different length-height scales

h=5 cm, exp.1

A. Velocity Field (m/sec):

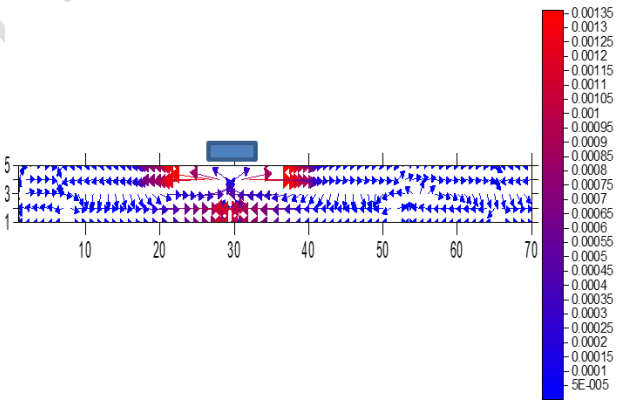

Figure 2. Results of the mathematical model-velocity field h=5 cm exp.1

B. Temperature field (^{0}C):

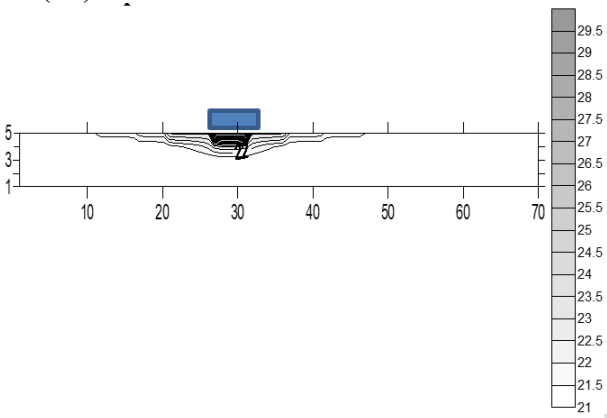

Figure 3. Results of the mathematical model - temperature field h=5cm exp.1

h=5 cm, exp.2

A. Velocity Field (m/sec):

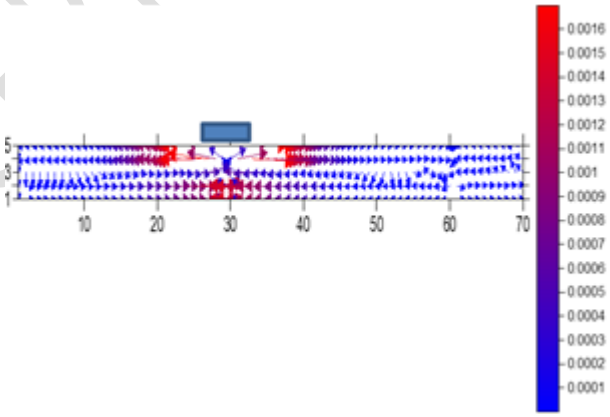

Fig. 4: Results of mathematical model-velocity field h=5 cm exp.2

B. Temperature field (^{0}C):

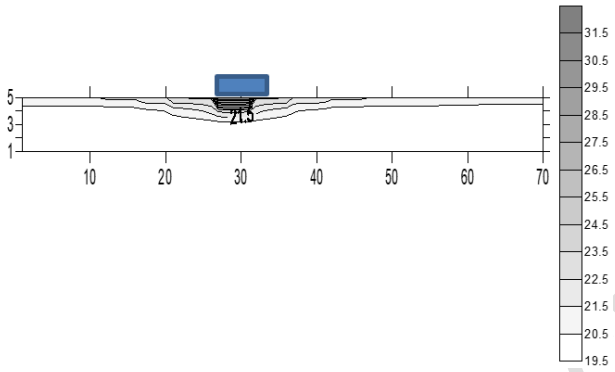

Figure 5. Results of a mathematical model - temperature field h=5 cm exp.2

h=5 cm, exp.3

A. Velocity Field (m/sec):

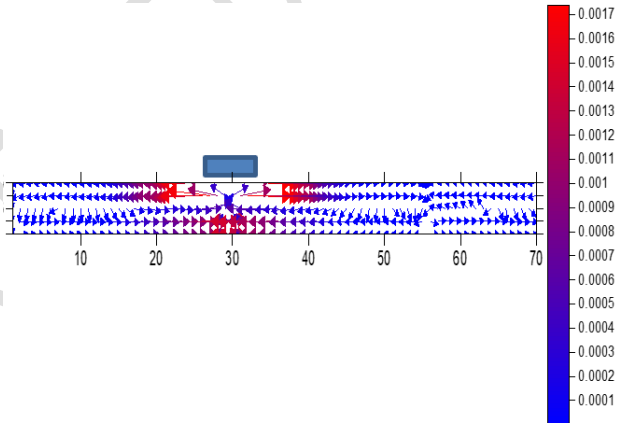

Figure 6. Results of mathematical model-velocity field h=5 cm exp.3

B. Temperature field (^{0}C):

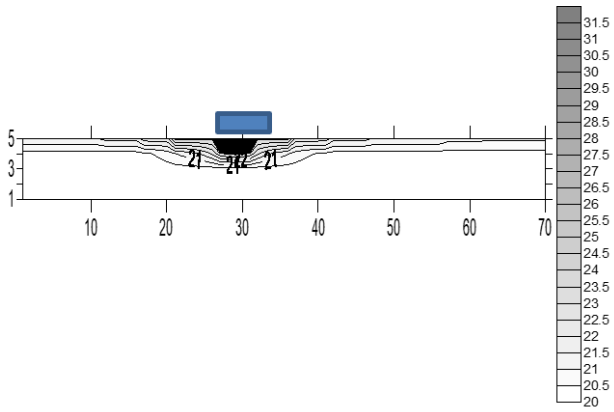

Figure 7. Results of a mathematical model - temperature field h=5cm exp.3

h=5 cm, exp.4

A. Velocity Field (m/sec):

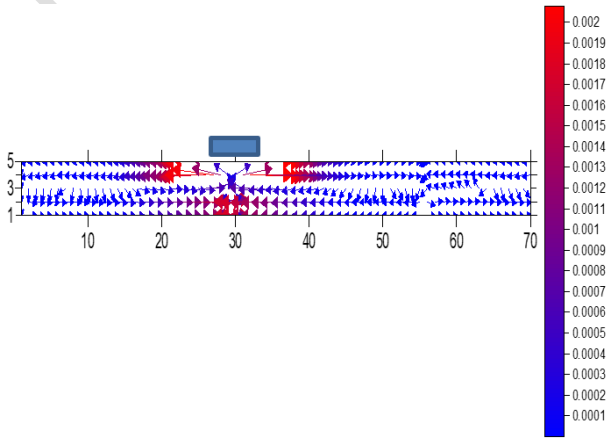

Figure 8. Results of mathematical model-velocity field h=5 cm exp.4

B. Temperature field (^{0}C):

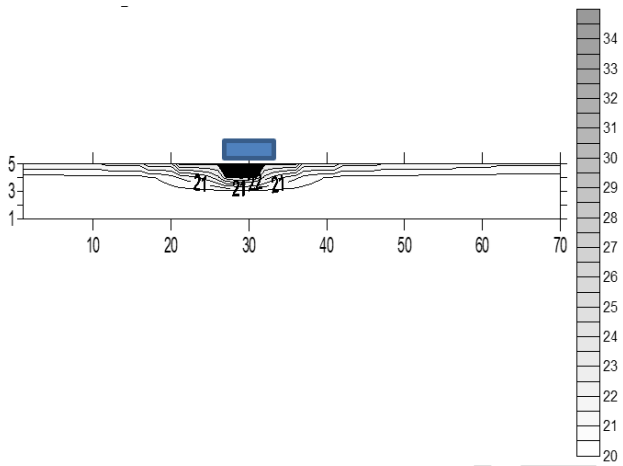

Figure 9. Results of a mathematical model - temperature field h=5cm exp.

h=5 cm, exp.5

A. Velocity Field (m/sec):

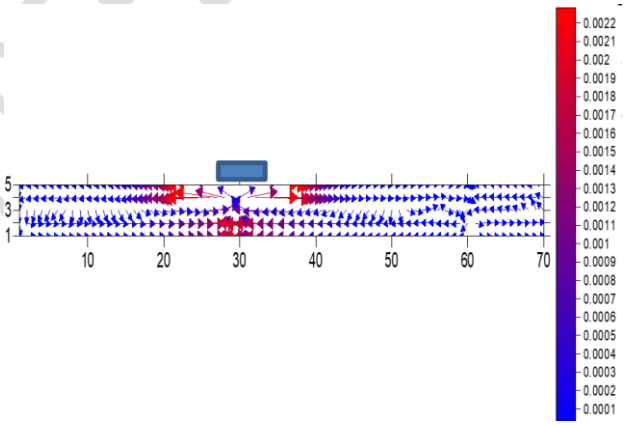

Figure 10. Results of mathematical model-velocity field h=5 cm exp.5

B Temperature field (^{0}C):

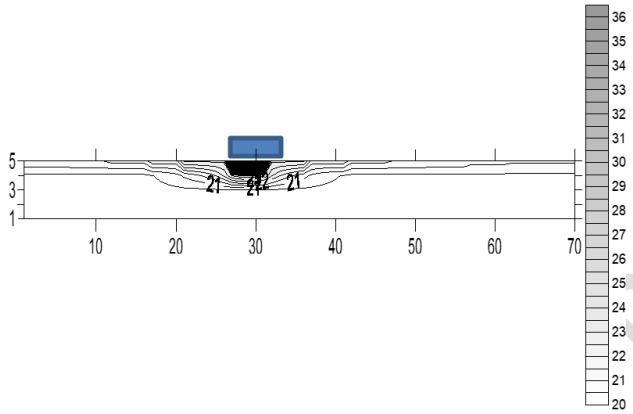

Figure 11. Results of a mathematical model - temperature field h=5 cm exp.5

h=15 cm, exp.1

A. Velocity Field (m/sec):

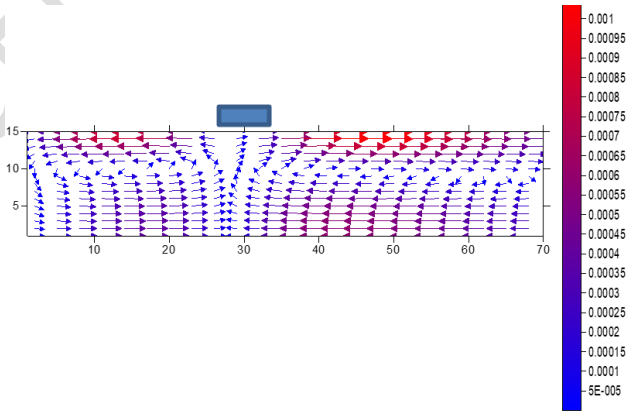

Figure 12. Results of mathematical model-velocity field h=15 cm exp.1

B. Temperature field (^{0}C):

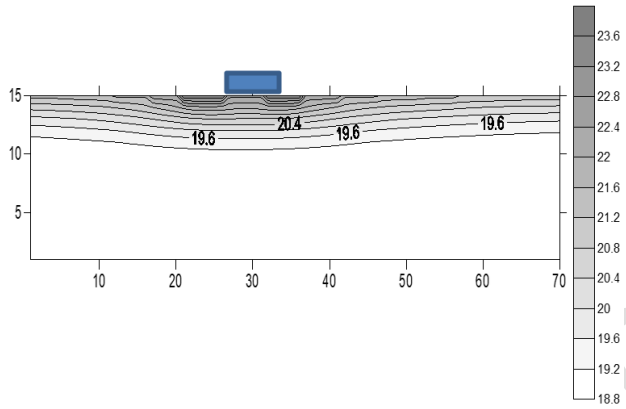

Figure 13. Results of a mathematical model - temperature field h=15 cm exp.1

h=15cm, exp.2

A. Velocity Field (m/sec):

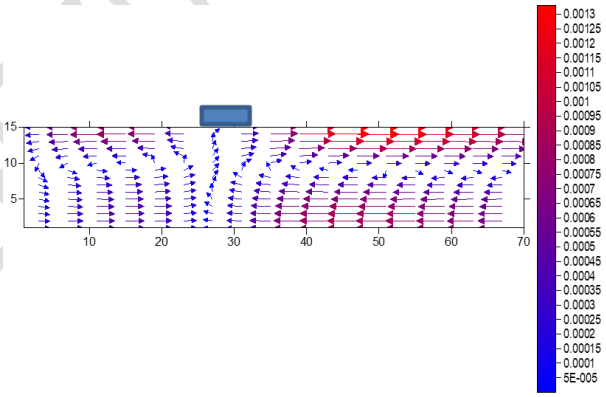

Figure 14. Results of mathematical model-velocity field h=15 cm exp.2

B. Temperature field (^{0}C):

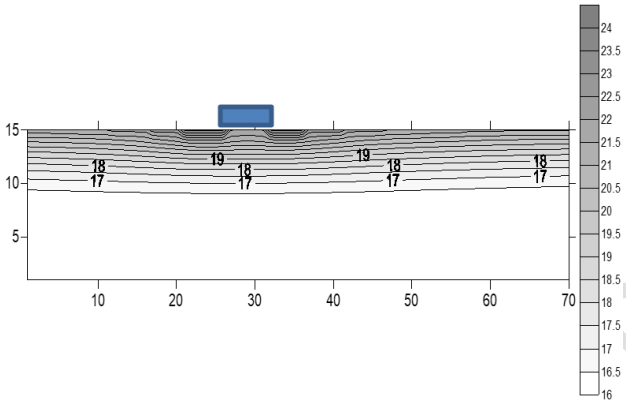

Figure 15. Results of a mathematical model - temperature field h=15cm exp.2

h=15 cm, exp.3

A. Velocity Field (m/sec):

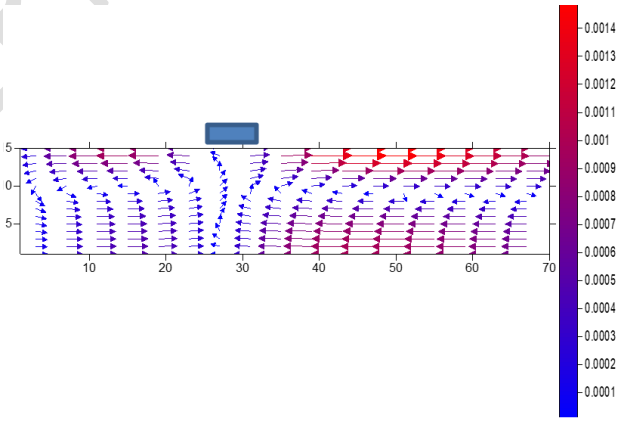

Figure 16. Results of mathematical model-velocity field h=15 cm exp.3

B. Temperature field (^{0}C):

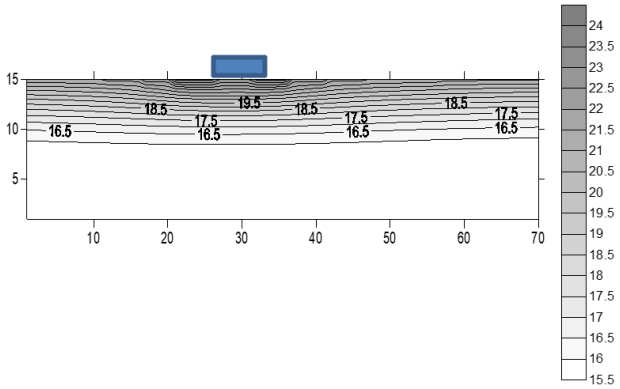

Figure 17. Results of a mathematical model - temperature field h=15 cm exp.3

h=15 cm, exp.4

A. Velocity Field (m/sec):

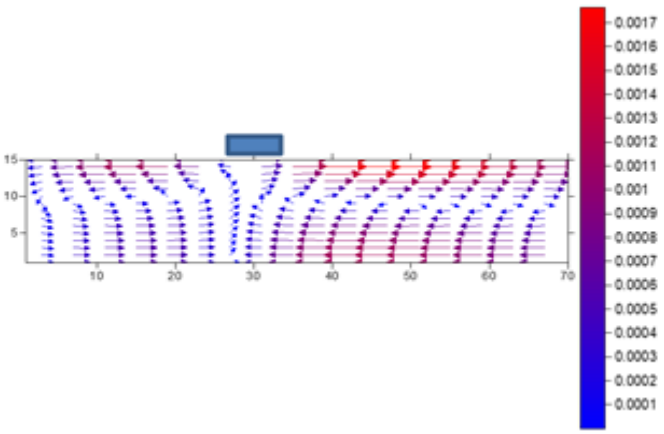

Figure 18. Results of mathematical model-velocity field h=15 cm exp.4

B. Temperature field (^{0}C):

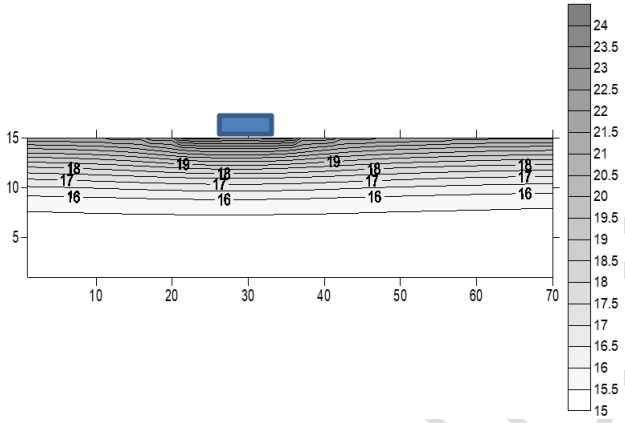

Figure 19. Results of a mathematical model - temperature field h=15cm exp.4

h=15 cm, exp.5

A. Velocity Field (m/sec):

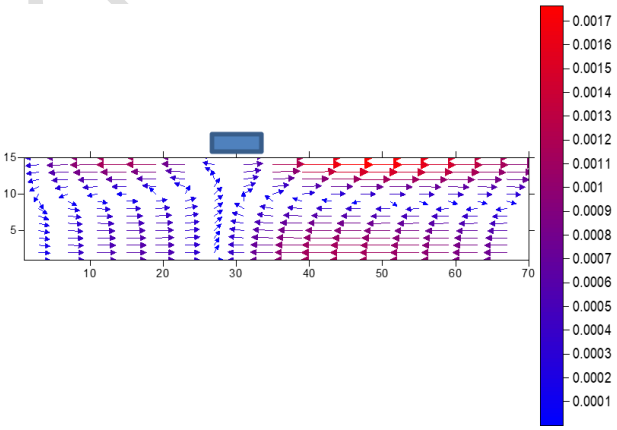

Figure 20. Results of mathematical model-velocity field h=15 cm exp.5

B. Temperature field (^{0}C):

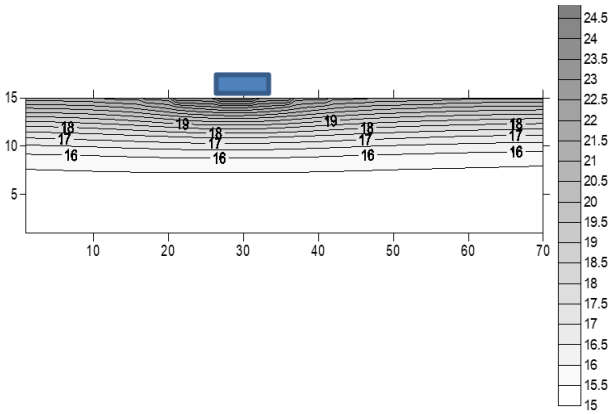

Figure 21. Results of a mathematical model - temperature field h=15 cm exp.5

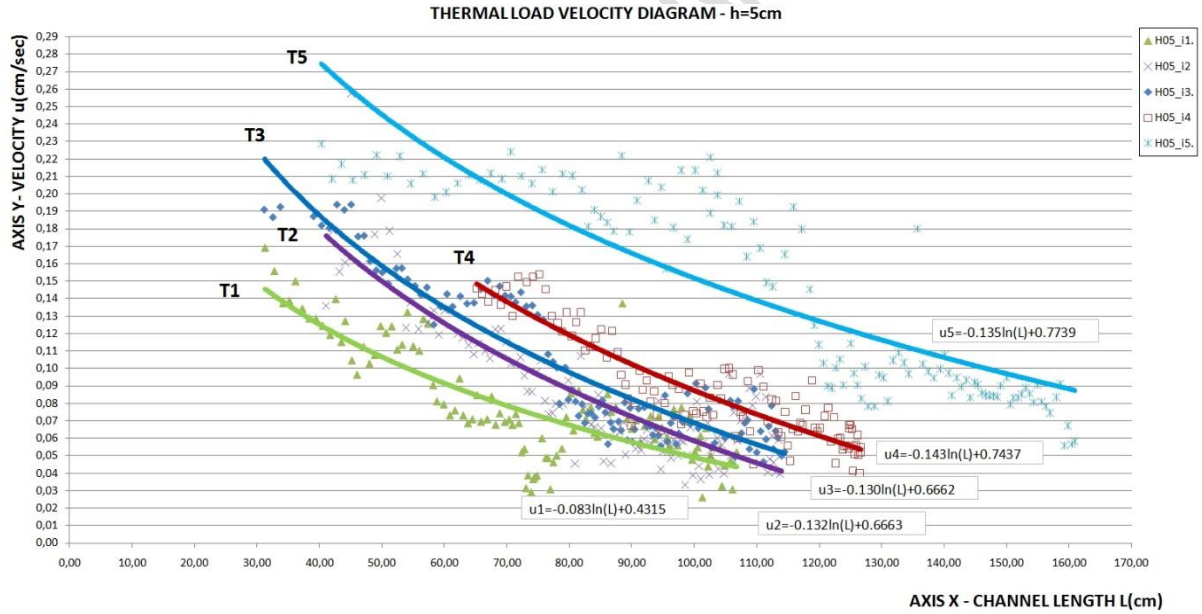

Figure 22. Experimental Mean velocity fields u (cm/sec) on the channel axis (X) for h = 5 cm

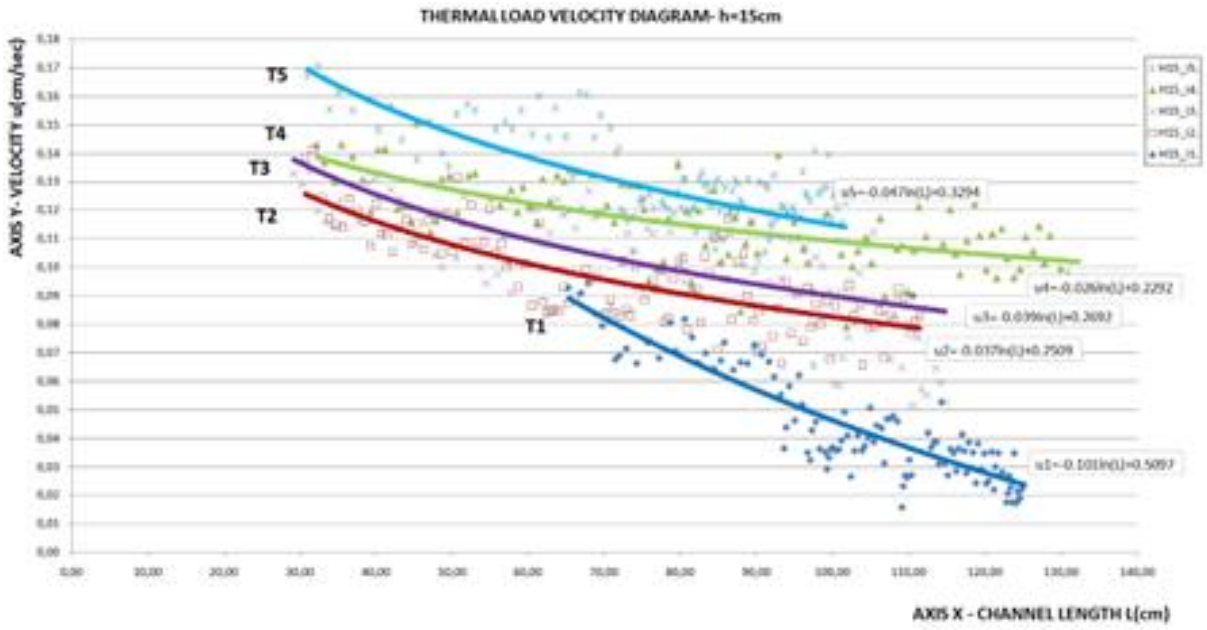

Figure 23. Experimental Mean velocity fields u (cm/sec) on the channel axis (X) for h = 15 cm

FLOW DEPTH 5cm

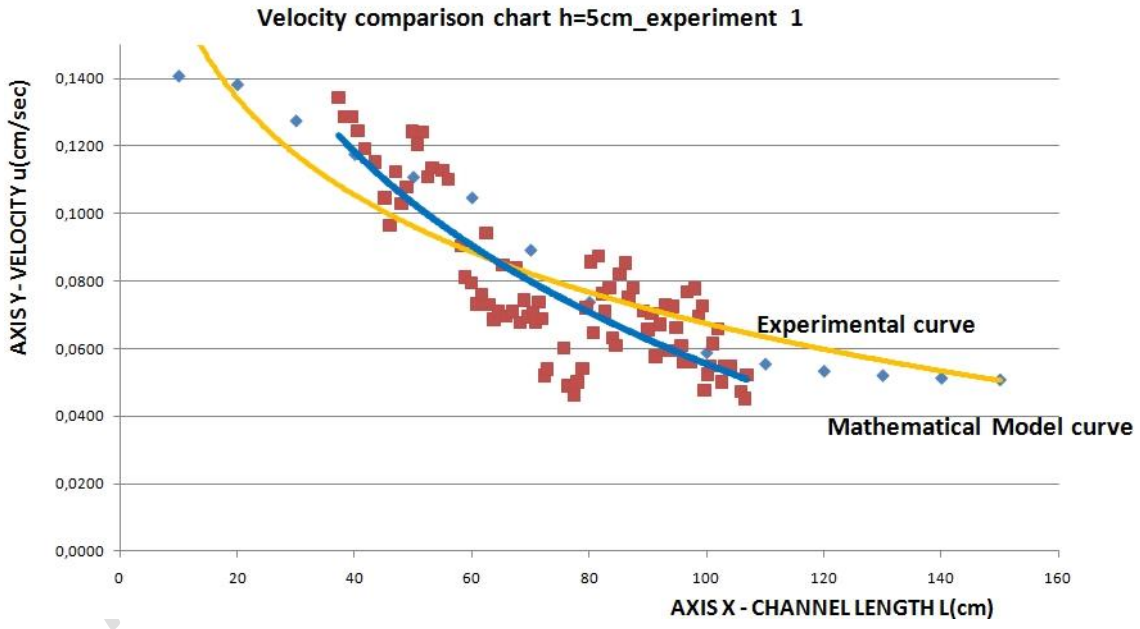

Figure 24. Depth h=5 cm, exp.1

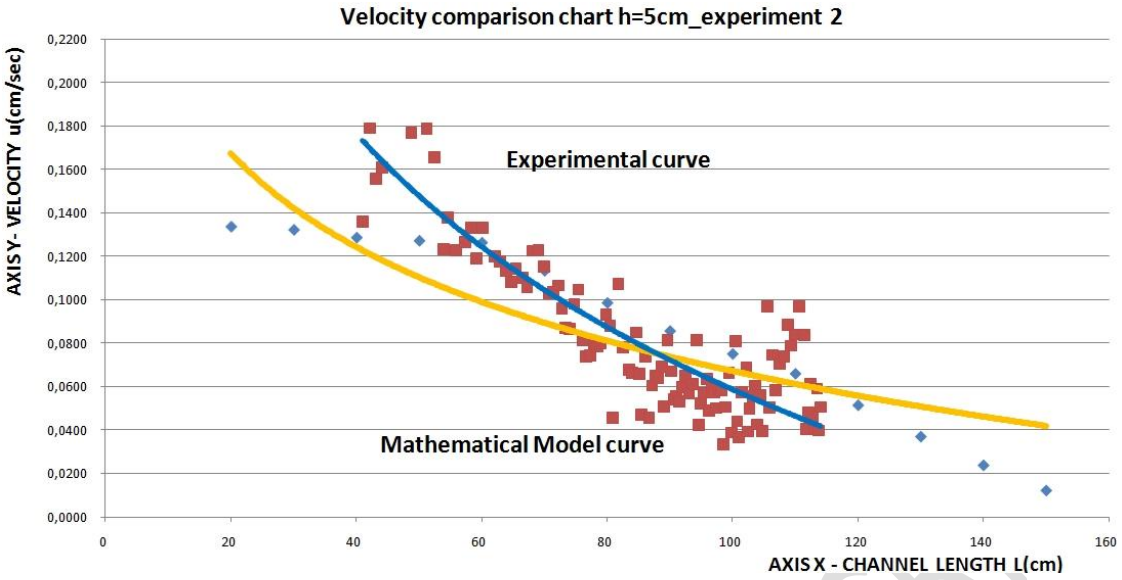

Figure 25. Depth h=5 cm, exp.2

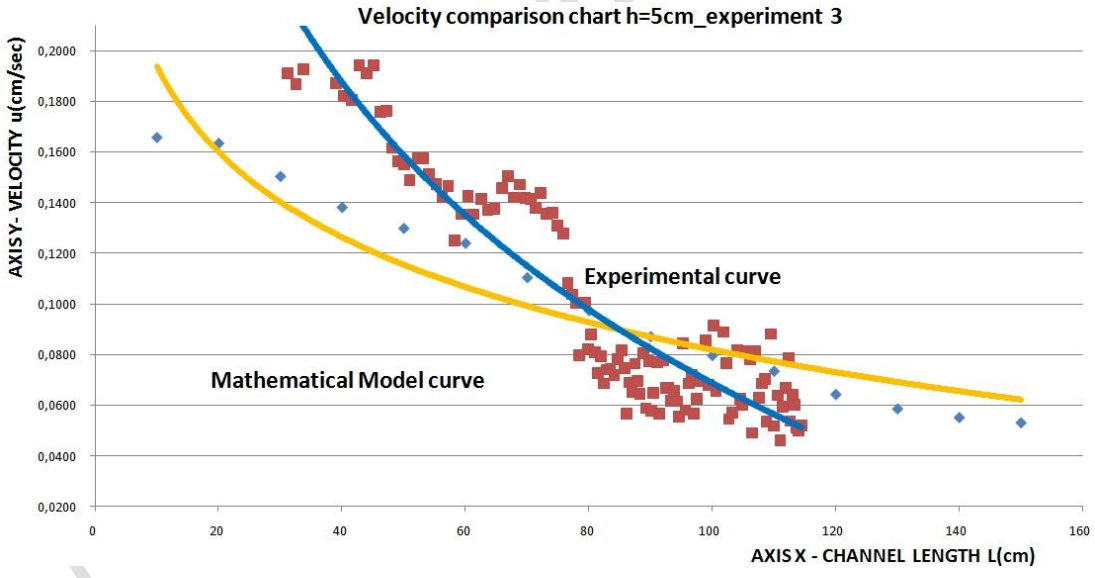

Figure 26. Depth h=5 cm, exp.3

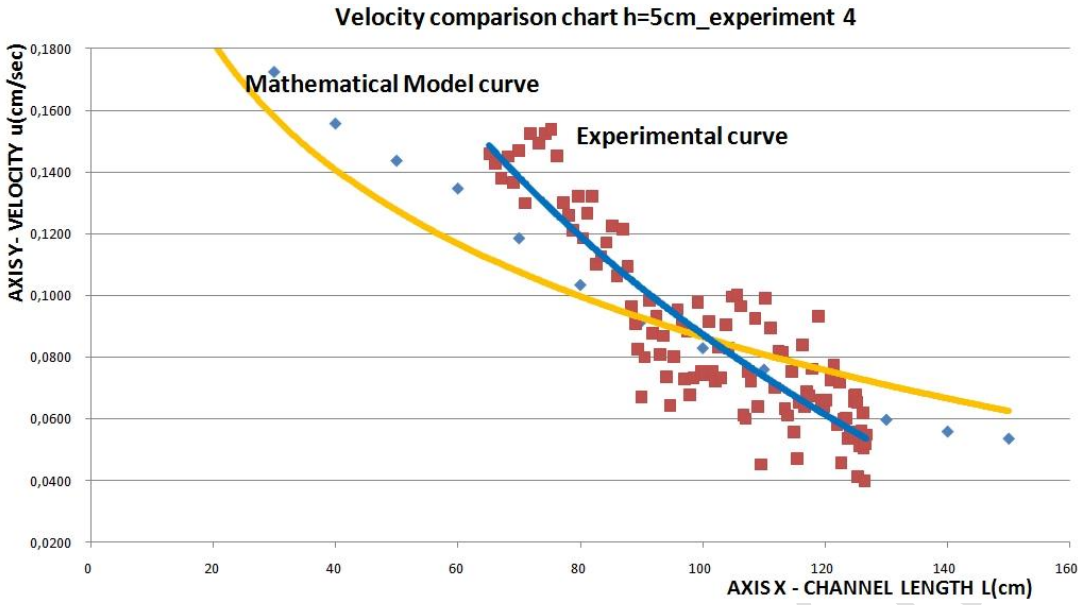

Figure 27. Depth h=5 cm, exp.4

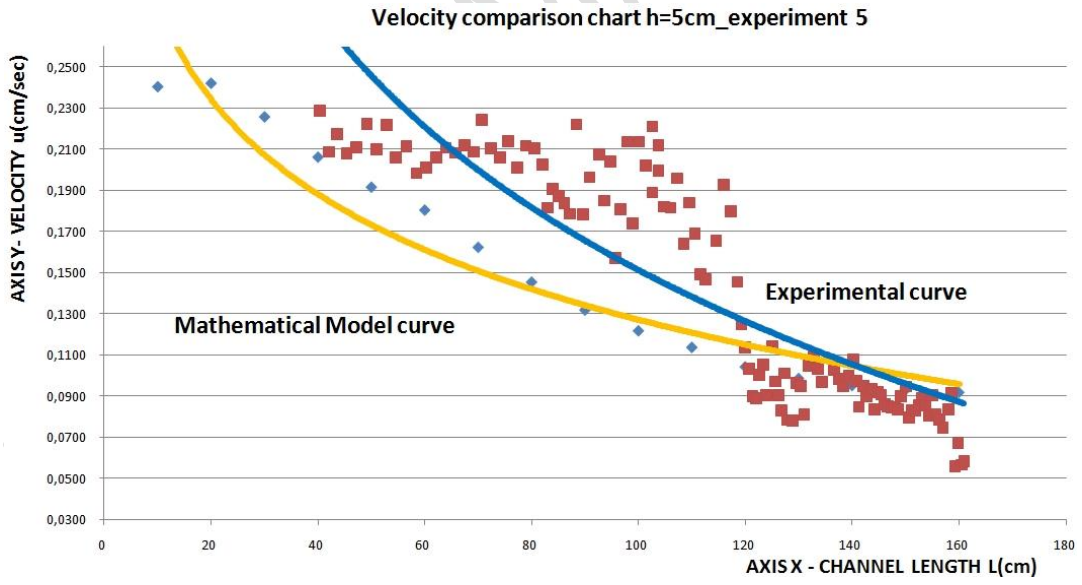

Figure 28. Depth h=5 cm, exp.5

FLOW DEPTH 15cm

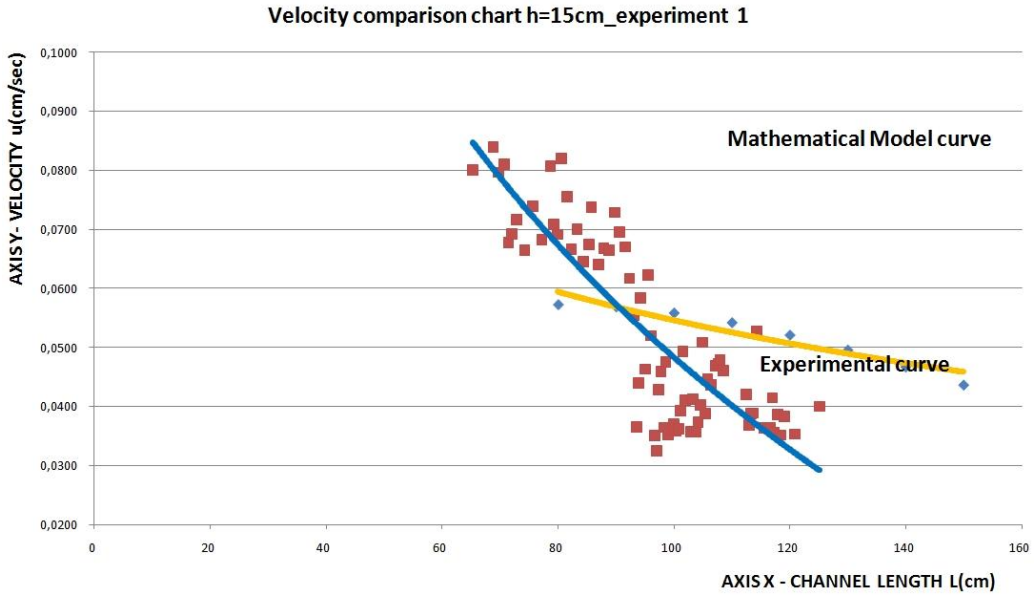

Figure 29. Depth h=15 cm, exp.1

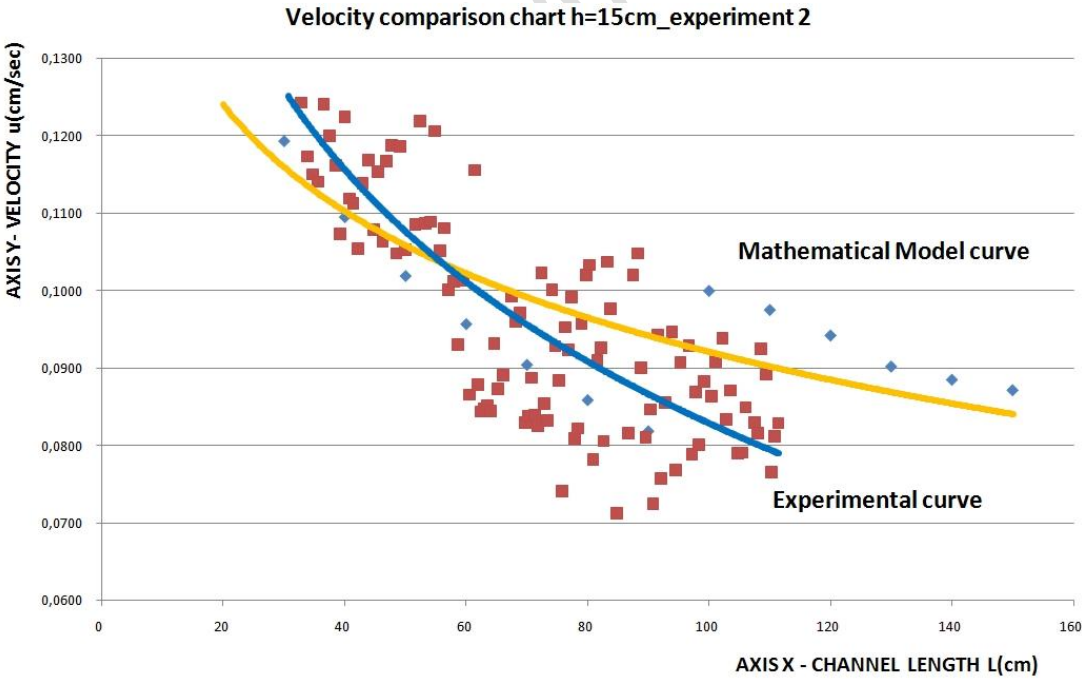

Figure 30. Depth h=15 cm, exp.2

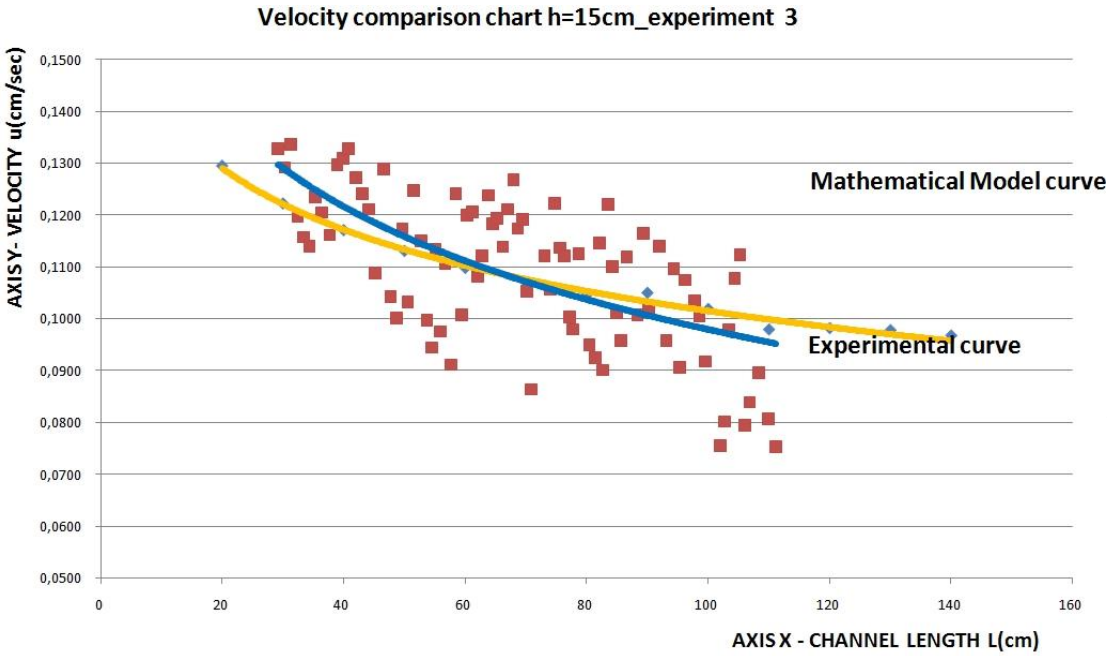

Figure 31. Depth h=15 cm, exp.3

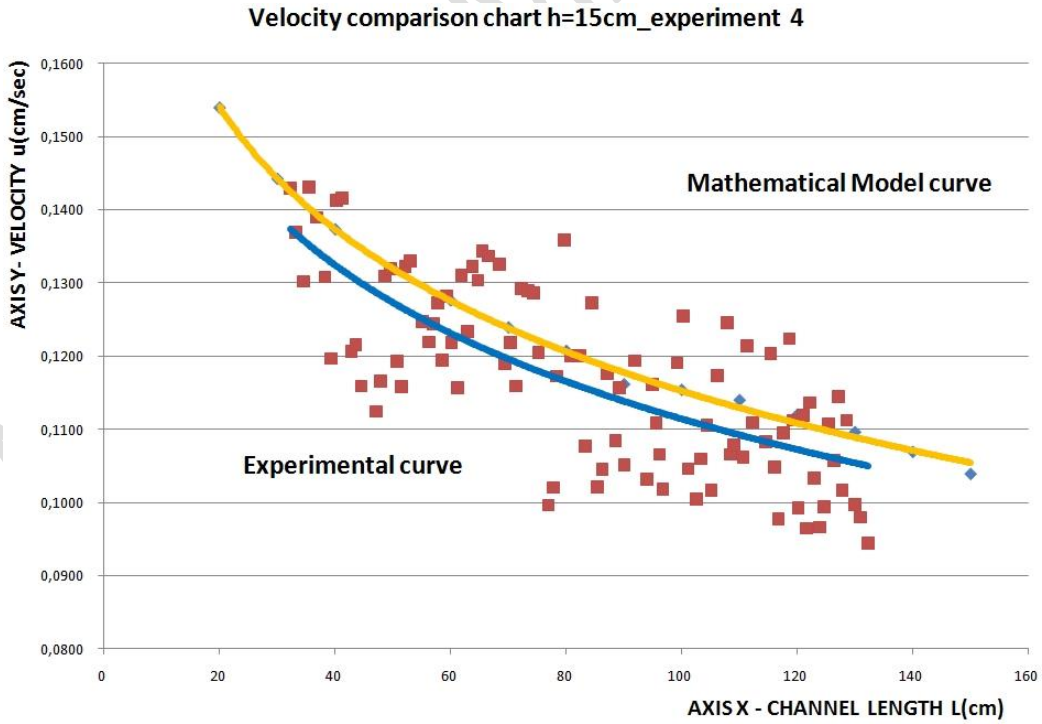

Figure 32. Depth h=15 cm, exp.

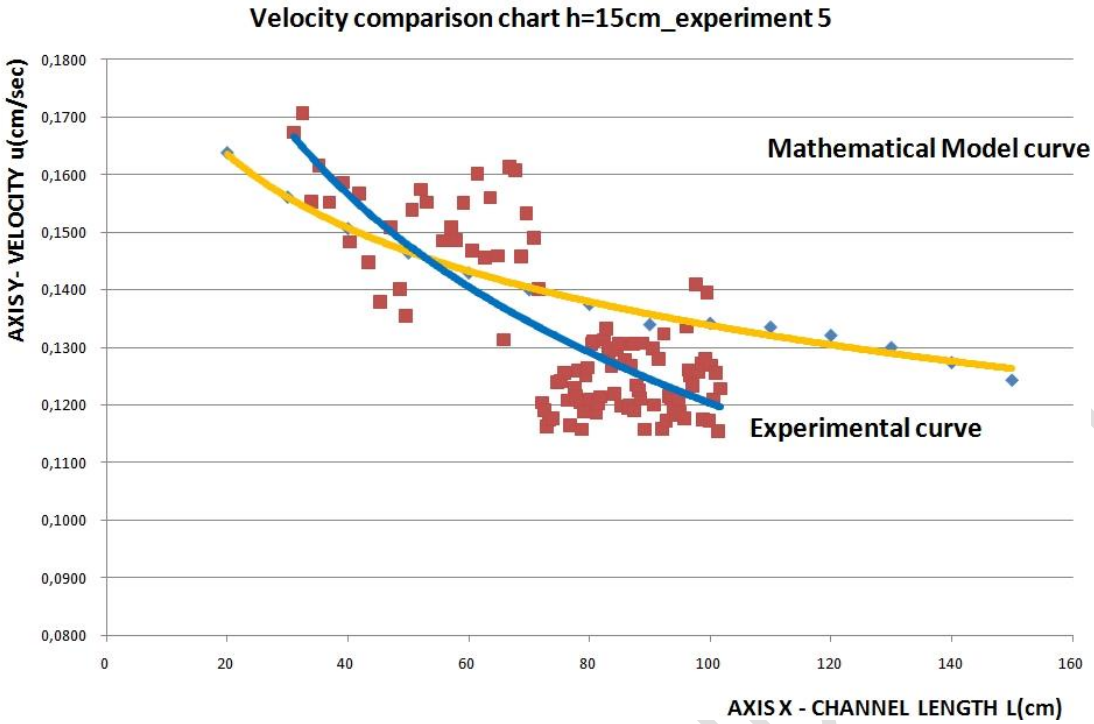

Figure 33. Depth h=15 cm, exp.5

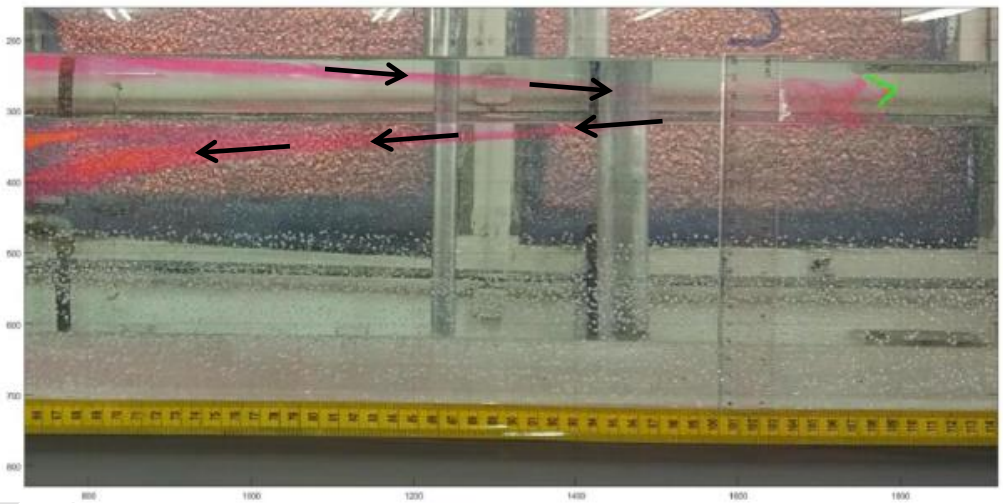

Fig. 34: Rhodamine's movement recorded experimentally. Black arrows were added for the better understanding of the phenomenon. The area of the channel corresponds to the part at the right side of the source.

Graphical Abstract

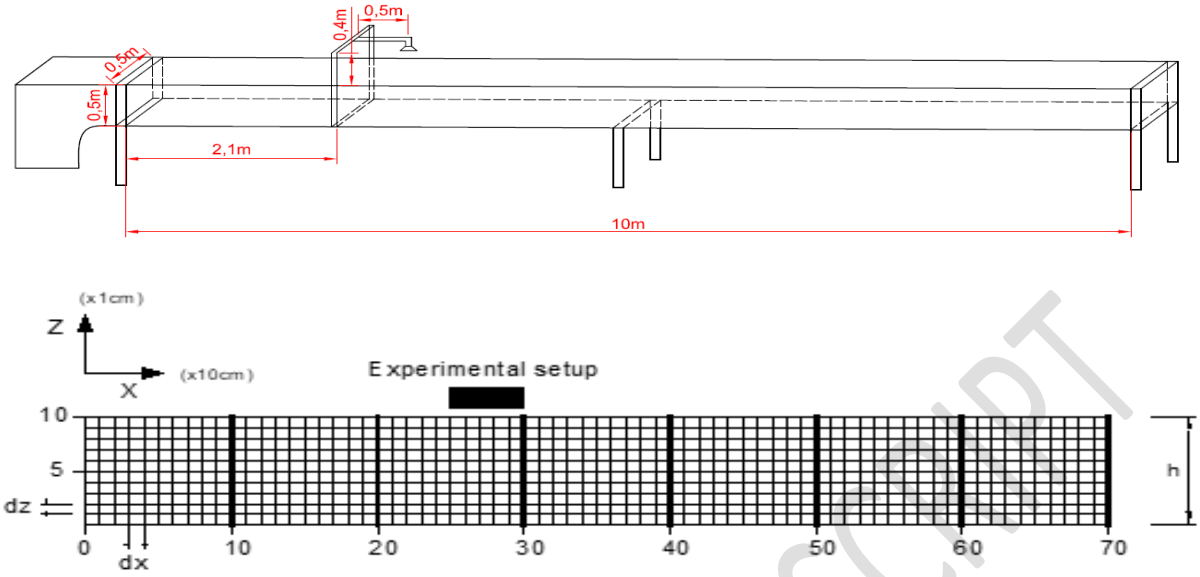

Schematic representation of calculation canvas generation with different length-height scales

Velocity Field (m/sec)

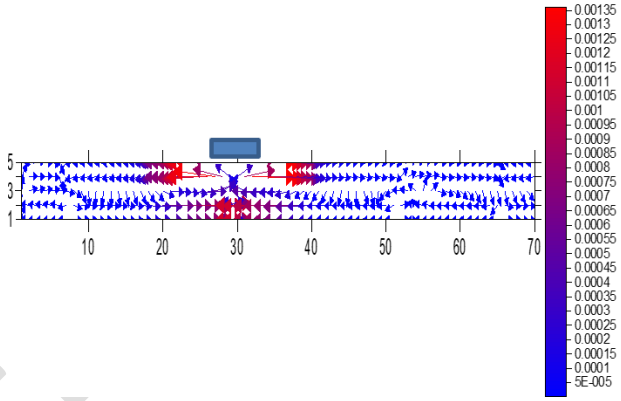

Results of the mathematical model-velocity field

Temperature field (^{0}C)

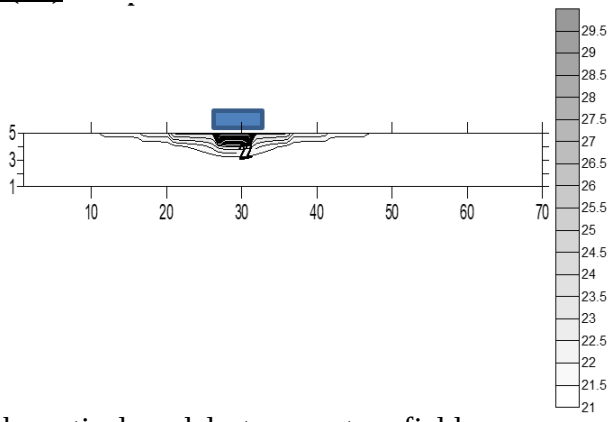

Results of the mathematical model - temperature field